Arabian Journal for Science and Engineering
https://doi.org/10.1007/s13369-019-04146-5

RESEARCH ARTICLE - EARTH SCIENCES

Geochemical and Petrographic Analyses of the Cambrian Oncoids of the North China Platform: Implications for Their Paleogeography and Paleoenvironment

Enzhao Xiao[1] · **Tehseen Zafar**[2] · **Khalid Latif**[1,3] · **Muhammad Riaz**[1] · **Yangbo Lu**[4]

Received: 22 May 2019 / Accepted: 13 September 2019

Abstract

After the global extinction event at the end of the Cambrian Epoch 2, widely spread oolitic bank dominated the North China Carbonate Platform during the Cambrian Miaolingian Epoch. To better understand the influence of paleogeographic and paleoenvironmental factors on microbial carbonate particles during this period, carbonate oncoids of the Cambrian Miaolingian Series were selected to reconstruct the paleogeography and paleoenvironment. The study samples were collected from four different sections: Wuhai, Diaoquan, Xiawidian and Sandaogou (from west to east in the North China Platform). Stratigraphic, sedimentological, petrological and geochemical studies including analysis of trace and rare earth elements were carried out to define the stratigraphic location, and morphological and geochemical characteristics of oncoids. Geochemical analysis of oncoids reveals that Er/Nd and Y/Ho values are relatively low, signifying that the formation of oncoids was influenced by terrestrial inputs. Meanwhile, Sr/Cu, Sr/Ba, V/Sc and V/Cr values indicate that the oncoids were developed in a shallow marine environment under oxidizing conditions. The low content of total rare earth elements, low LREE/HREE ratios and LREEs, negative anomalies of Ce/Ce* and Eu/Eu* as well as $(La/Sm)_N$ suggest that the oncoids were less influenced by late diagenetic processes. More importantly, morphological differentiations of oncoids in the study area coincide with the changing trend of Y/Ho and Sr/Ba. The results of this study show that oncoids with regular morphology mainly formed at offshore area, while those with irregular shape and preserving rough laminae mostly occurred at nearshore area. From the comparison made between the paleogeographic locations of the study sections, it is proposed that the paleosalinity of marine depositional environment and the transportation distance are the prime controls for morphological differentiation of oncoids.

Keywords Oncoids · Trace element · Rare earth element · Miaolingian Series · North China Platform

1 Introduction

“Oncoids” as a non-genetic term was firstly introduced by Heim [1] to describe the micrite particles found in the Jurassic shelf limestone in Switzerland [2]. Researchers report them as typical carbonate particles and independent calcareous or non-calcareous nodules, having circular or ellipsoid shapes with millimeter to centimeter range of grain size and concentric structure [2–8]. These grains are widely studied at temporal and spatial scales, ranging from Precambrian to modern in age [7, 9–18]. Although the genetic interpretation of different types of oncoids differs, owing to their diversity of forming environment and mineral compositions, a common understanding of their biogenicity has been achieved in the previous century [2].

The formation process of oncoids is revealed by their structures and frameworks including development of

✉ Muhammad Riaz
riazjass@yahoo.com

[1] School of Earth Sciences and Resources, China University of Geosciences, Beijing 100083, China

[2] Institute of Geochemistry, Chinese Academy of Sciences, Guiyang 550081, China

[3] National Centre of Excellence in Geology, University of Peshawar, Peshawar 25130, Pakistan

[4] Key Laboratory of Tectonics and Petroleum Resources of Ministry of Education and Faculty of Earth Resources, China University of Geosciences, Wuhan 430074, China

Published online: 26 September 2019

nucleus, concentric laminae and morphological characteristics of cortex [19]. The process of oncoids development is governed by paleogeographic and paleoenvironmental factors (more specifically water and atmospheric chemical conditions) that are governed by the sea level changes [20, 21]. Furthermore, the variance of morphological characteristics of the oncoids is primarily dependent on the stability of sedimentary environment [22]. Therefore, oncoids are not only used as an indicator of regional stratigraphic division and correlation, but also as an essential marker for paleogeographic reconstructions [15–18, 20, 21, 23]. Therefore, the study of morphology and origin of oncoids can provide notable implications to explore their paleogeography and paleoenvironment [15, 24, 25].

The oncoids from Cambrian strata of the North China platform have been reported for genetic discussions and growth models [6, 7, 16, 17, 25–27]. However, the comprehensive morphological characteristics and large-scale comparative study of the oncoids exposed in different areas of the North China Platform are still lacking. Furthermore, the trace element geochemistry of these oncoids to delineate the paleoenvironmental conditions is yet unexplored. Therefore, we integrated the lithological, morphological, sedimentological and geochemical (trace elements and rare earth elements) features of great varieties of oncoids in a wide range. This study is aimed at systematically demonstrating the intrinsic relationship between the morphological variations of oncoids and paleoenvironmental factors through the geochemical clues.

2 Geological Setting and Sequence Stratigraphic Framework

2.1 Geological Background

The study area is located in the northern part of the North China Platform (ca. 1000 km north–south, 1500 km east–west; [28]) (Fig. 1). From the Cambrian Epoch 2 through the middle of Ordovician, the sediments of the North China Platform were dominated by epicontinental sea sediments [29]. Samples of the present study were collected systematically from the Cambrian strata in four different locations, which can be categorized in sequential orders including: A—Wuhai (Inner Mongolia Province), B—Diaoquan (Shanxi Province), C—Xiaweidian (Beijing), and D—Sandaogou, Huludao (Liaoning Province). The locations of these exposed sections of the North China Platform are illustrated in Fig. 1. All oncolitic samples were taken from the Xuzhuang and Zhangxia formations of the Miaolingian Series.

Within the new chronostratigraphic framework [32, 33], the Miaolingian Series strata of Cambrian (509–497 Ma) contain the Maozhuang, Xuzhuang, Zhangxia and Gushan formations [34–38], which are characterized by massive oolitic–grain bank facies (Fig. 2). The basic sedimentary characteristics of the Xuzhuang Formation are evaporative red beds in the lower part and dark calcareous mudstone in the middle part. From the middle to the top, deposition occurred in a shallowing upward environment, and the formation is dominated by banded and massive limestone to oolitic limestone (Fig. 2). The Zhangxia Formation as a whole is believed to have deposited in a third-order depositional sequence [34–38]. According to its lithological characteristics and cyclicity of sedimentary facies at different levels, Zhangxia Formation can be subdivided into three fourth-order sequences, and all of them are marked by shelf facies calcareous mudstone in the lower parts. The middle parts are composed of banded mudstone interbedded with thin beds of oolitic limestone, and the upper parts are composed of massive oolitic limestone. The variation in the internal lithologic characteristics of the Zhangxia Formation reveals a cyclicity change from non-grain bank to grain bank facies and deep water to shallow water environments, as well as a shallowing upward trend in the deposited sediments. The Gushan Formation in the studied section exhibits one third-order sequence that is marked by mudstone at the bottom, alternating marl and banded limestone in the lower-middle part and alternating massive limestone and oolitic limestone in the upper part [34, 35].

Stacked patterns of the formations, vertical variations of sedimentary facies and characteristics of the inner cycle, suggesting three or four third-order sequences, were developed in these sections (Fig. 2). In the description of the Cambrian paleogeography of the North China Platform by previous researchers, the entire terrain of western margin of the Yimeng and Lvliang regions remained steeper than the eastern margin during the Cambrian [28, 29]. Hence, the Cambrian sedimentary sequence of the Wuhai section reflects deeper water environment in comparison with the three eastern sections. The strata in Wuhai section are thinner with decreased thickness of limestone, while increased thickness of mudstone (Fig. 2).

2.2 Sequence Stratigraphic Framework of the Cambrian Miaolingian in the North China Platform

According to the new framework of the Cambrian strata, vertical variations in the trends of sedimentary facies within a cycle and deposition in three or four third-order sequences (controlled by third-order sea level changes, with a cycle frequency of 0.5–3 Myr) [34, 35, 39] can be interpreted for these specific sections (Fig. 2). The oncoid-bearing intervals in Wuhai and Xiaweidian sections are all located in the Xuzhuang Formation, while

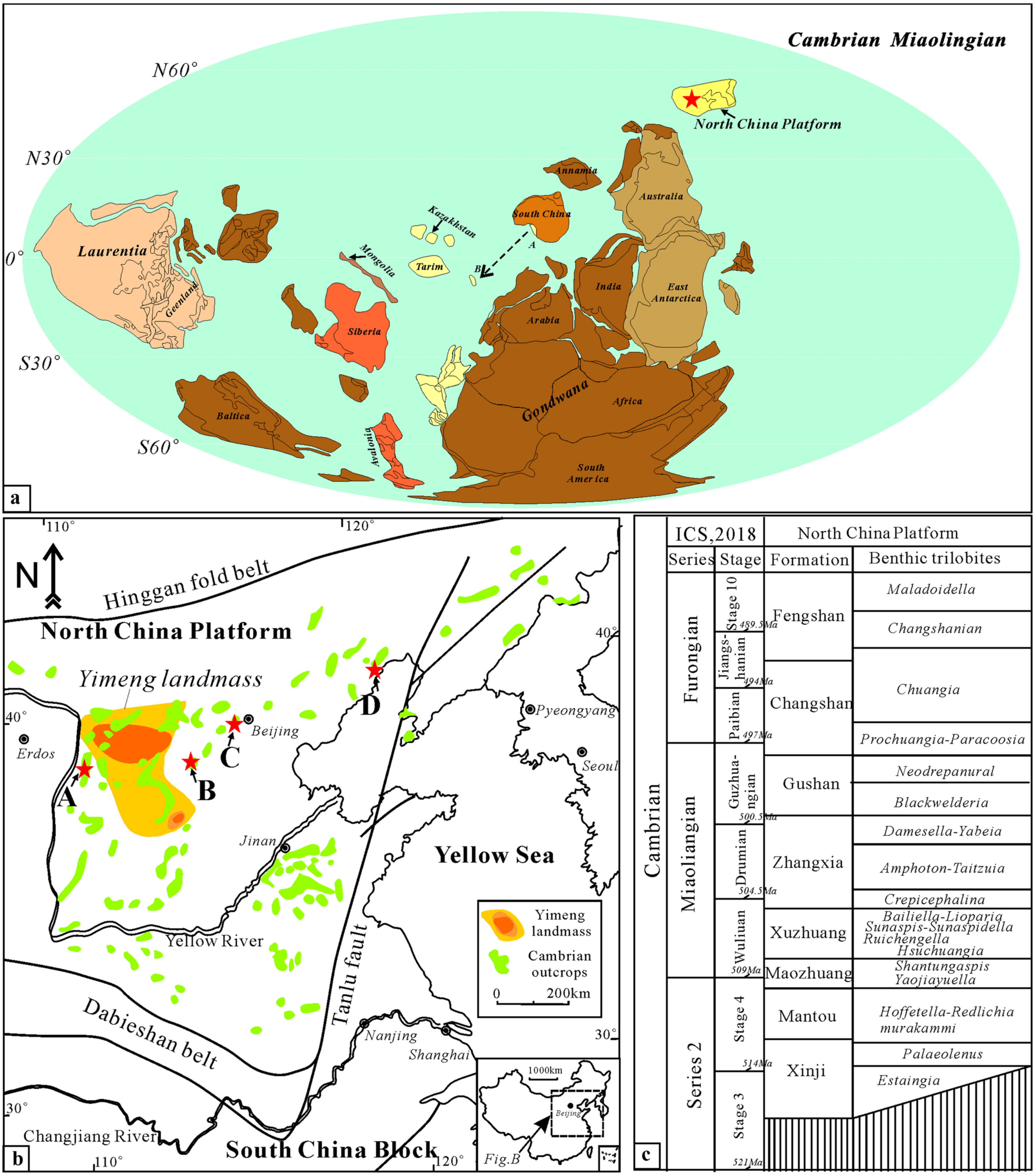

Fig. 1 **a** Global location of the Cambrian Miaolingian Series in the North China Platform; **b** geological setting of Cambrian outcrops in the North China Platform and the study area locations (Red Stars: A—Wuhai section, B—Diaoquan section, C—Xiaweidian section, D—Sandaogou section); **c** Cambrian stratigraphic successions in the North China Platform and their correlation with the international chronostratigraphic subdivisions [30–32]

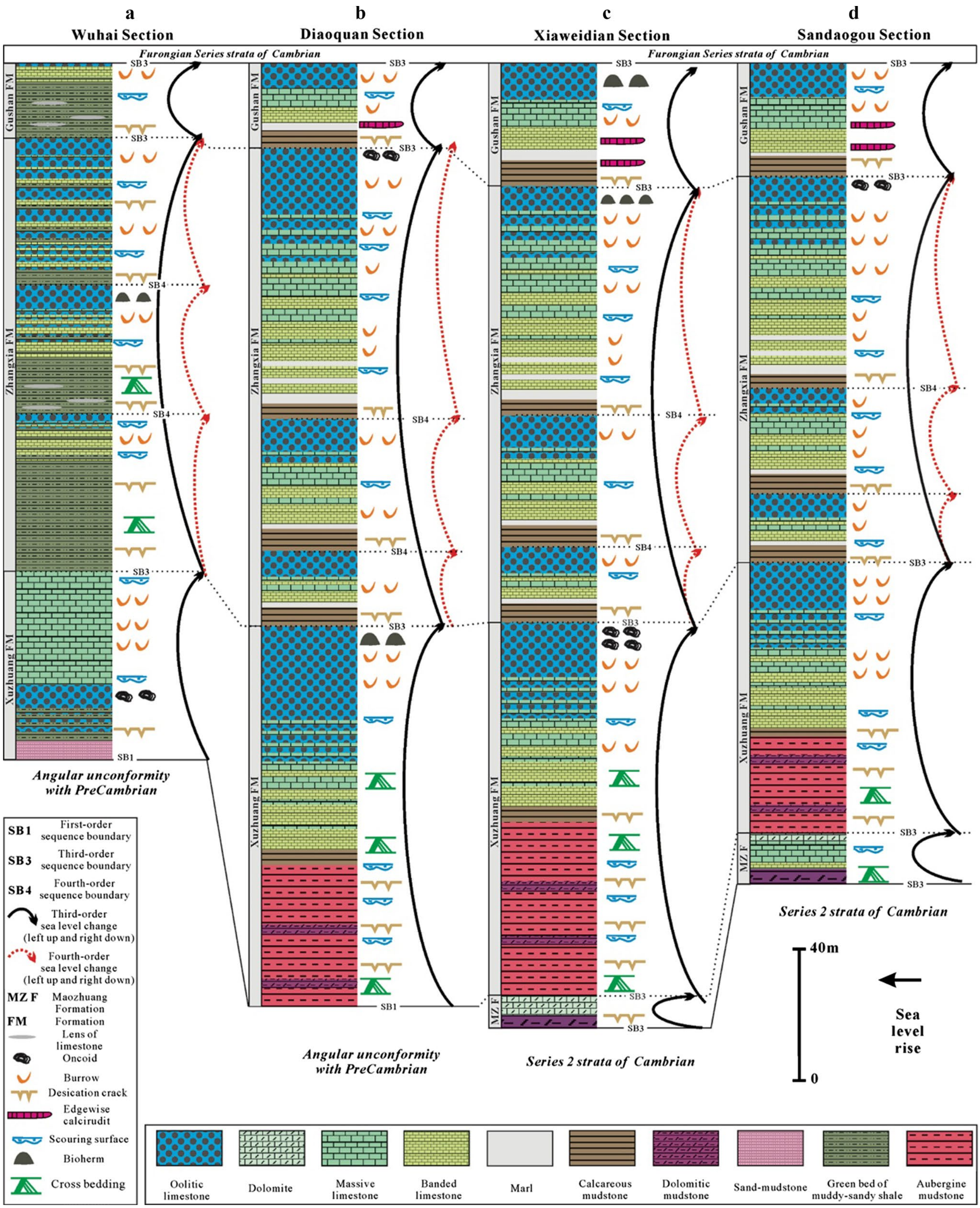

Fig. 2 Sequence stratigraphic framework of the Cambrian Miaolingian Series strata from A to D section [34, 35], third- and fourth-order sea level changes and locations of oncoids occurrences

those in the Diaoquan and Sandaogou sections are all located in the Zhangxia Formation. According to the vertical variation of sedimentary facies and the cyclic characteristics of lithology in each section, the Xuzhuang Formation displays a third-order depositional sequence in the stratigraphic framework. The prevailing lithologies of the Xuzhuang Formation are evaporative red beds in the lower part and dark calcareous mudstone in the middle part. From middle to upper part, the depositional settings of the formation are characterized by shallow marine environment, featured by the widespread banded and massive carbonates to oolitic limestones (Figs. 2, 3). In contrast, the Zhangxia Formation as a whole forms an individual third-order depositional sequence. It can be further subdivided into three fourth-order sequence. The middle parts of these subsequences are characterized by interbedded banded mudstone and thin beds of oolitic limestone. Massive oolitic limestones were observed in the upper parts. In addition, the top and bottom peripheries of these subsequences denote typical sequence boundary of drowning unconformity type and rapid sea level rise [34–38].

3 Materials and Methods

The current study is based on field observations, field measurements and laboratory tests on 442 oncolitic–oolitic limestone samples collected from the Miaolingian strata exposed along the four sections (Figs. 2, 3). Lithological column for the exposed strata of the Miaolingian Series was reconstructed on the basis of field and laboratory studies. Fresh, representative samples of oncoids were systematically collected from the Xuzhuang and Zhangxia formations which were examined at mega-, macro-, meso-, micro- and ultramicro-scales. Microfacies observation (XPL and PPL) was accomplished on polished samples and thin sections to observe the key lithological and paleontological components. Scanning electron microscopy (SEM) analyses were performed on polished sections and freshly broken surfaces at the micron scale.

In addition, inductively coupled plasma–mass spectrometry (ICP–MS) analysis was performed on micro-drilled samples. Fresh samples were collected from areas without noticeable weathering. These particular samples were also observed under microscope to avoid calcite veins and neomorphic processes. Observations revealed a complete absence of secondary features. The samples of oncolitic

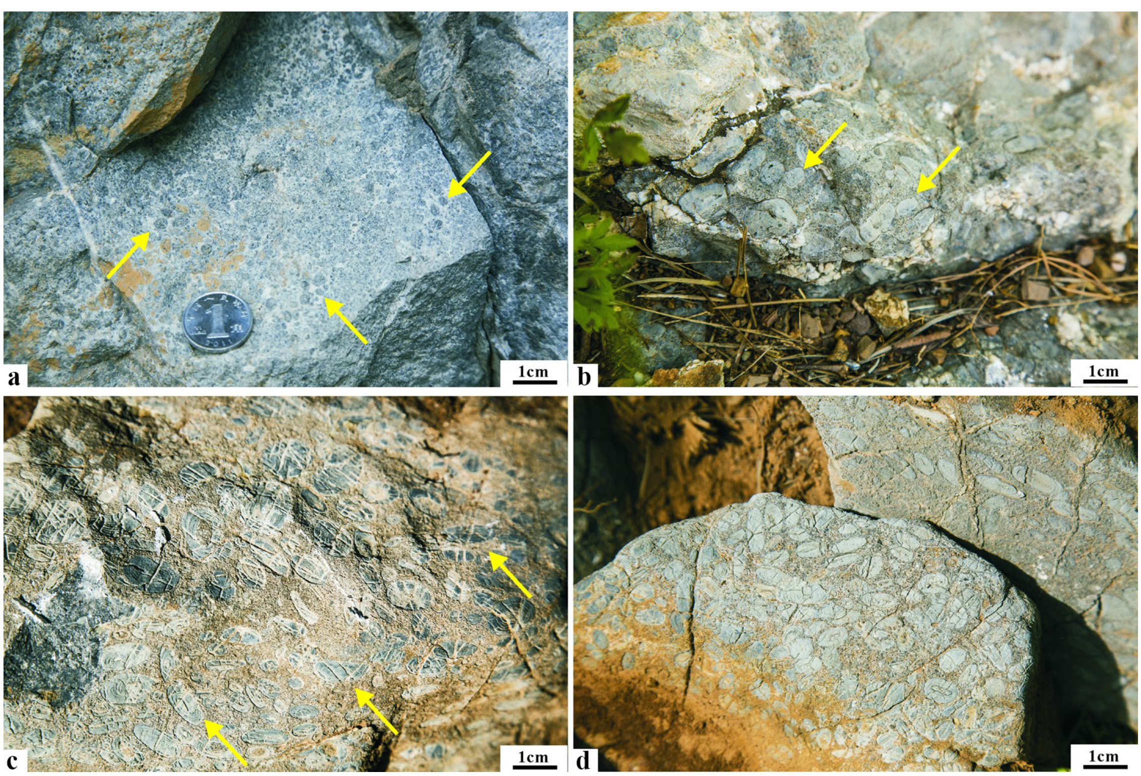

Fig. 3 Macroscopic characteristics of oncoids from various sections of Cambrian Miaolingian Series. **a** Oncoids from Wuhai, Xuzhuang Formation; **b** oncoids from Diaoquan, Zhangxia Formation; **c** oncoids from Xiaweidian, Xuzhuang Formation; **d** oncoids from Sandaogou, Zhangxia Formation (yellow arrows show the oncoids from outcrop in the field)

limestone were cleaned off the weathered surficial layer, and the part without fractures and alteration was chosen for the analyses. Sample chips of 1 cm cube without diagenetic and weathering features were selected for geochemical analyses. Trace elements in rock samples were analyzed by ICP–MS. The detection limits of rare earth elements and other trace elements are 0.01×10^{-6}–0.5×10^{-6} and 0.5×10^{-6}–10×10^{-6}, respectively. The accuracy of analysis meets or surpasses the national standard, and the results are presented in Table 1. All geochemical analyses of oncolitic samples were performed in the State Key Laboratory of Oil and Gas Geology and Exploitation, Chengdu University of Technology.

4 Results

4.1 Sedimentary Features of Oncoids

4.1.1 Macro- and Micro-characteristics of Oncoids

The thickness of oolitic limestone with oncoids is measured in the range of 0.3–5 m and documented as layered, interbedded with thinly layered micritic limestone. The oncoids exhibit ellipse or strip shape with a major axis length of approximately 0.3–2.1 cm (Fig. 3). In context of sequence stratigraphy, all varieties of oncoids occur at the top of third-order sequence. Some differences in these oncoids can be witnessed macroscopically. For example, volume and diameter of oncoids in the Wuhai section (section A) are prominently smaller in comparison with other sections. Likewise in this section, the oolitic limestone layer with oncoids growth in the Xuzhuang Formation is fairly thinner in contrast to beds of oncoids in the Xuzhuang Formation in sections B, C and D. The oncolite layer in the Zhangxia Formation of Diaoquan section is typically smaller compared with those of the Sandaogou section.

The microscopic observations of oncoids from the four sections depict development of oncoids together with ooids. The individual size of oncoids varies, and their shapes are circular to sub-circular. Most of the oncoids display the presence of nucleus, that is featured by inclusion of dark micrite, trilobite bone or echinoderm bioclast. Moreover, most of the oncoids are defined by alternating traits of light and dark laminae, which can be specified as spherical stromatolites [2]. The light laminae are composed of sparite or microspar, and the dark laminae consist of micrite. Besides this, filamentous cyanobacteria fossils, mainly *Girvanella*, can be identified in the interlaced layer or inside the interior and core of the oncoids laminae (Fig. 4).

Based on petrographic observations regarding the development of nucleus and lamina, location of nucleus and morphological attributes, the oncoids can be subdivided into eight groups including concentric fine laminar, concentric rough laminar, lateral growth, micritic, multicore, complex basement, flaggy and thin-cortex oncoids (Fig. 4). Moreover, typical filamentous cyanobacterial fossils, especially *Girvanella* [40–42], are abundant in addition to microbial-related precipitates (pyrite) [43] (Fig. 4).

4.1.2 Ultramicroscopic Characteristics of Oncoids and Mineral Composition of Lamina

As obvious from morphological characteristics of oncoids from Miaolingian Series, the oncolites can be classified into eight types. According to SEM observation of oncoids, a common characteristic of bimineralic structure exists in oncoids containing microspar and micrite laminae. The ultrastructure image of dark laminae composited by micrite reveals distinct mineralogical structure (Fig. 5a, b).

The micrite structure is associated with carbonate mud of microbial origin which is consistent with the findings of previous studies [2]. Moreover, pyrite grains (Fig. 5c) are also witnessed in dark micrite. The present study documents two types of pyrite, one is ordinary massive pyrite and the other is framboidal pyrite (Fig. 5c). The occurrence of framboidal pyrite represents one of the microbial genetic evidences of the oncoids, which is associated with sulfate-reducing bacteria and stimulates the microbial metabolism of carbonate precipitation [42, 43].

Besides this, the most noticeable phenomenon from the observation of dark micrite under SEM involves large numbers of exquisitely preserved microbial fossils and some microbial-related structures, such as EPS calcification remnants and nanospheres (Fig. 5). In particular, the types of microbial fossils include spherical calcified (Fig. 5d–g), filamentous (Fig. 5h, i) and rod-like microbial fossils (Fig. 5j, k). This implies that the dark laminae of oncoids can be reflected as calcification products of microbial community (microbial mat or biofilm) [7].

4.2 Geochemical Characteristics of Oncoids

4.2.1 Trace Elements

Variations in the oxidation–reduction conditions of depositional environment can lead to loss or enrichment of redox-sensitive trace elements in the sediments [44]. Hence, the redox conditions of depositional settings can be reconstructed using a variety of trace elements present in carbonates of the North China Platform. The varieties of rare earth elements and other trace elements of oncoids are displayed in Figs. 6, 7 and Table 1.

V, V/Sc, V/Cr and V/(V + Ni) are significant to determine the redox characteristics of sedimentary environment [45–47]. Low V/Cr ratio (<2) is indicative of

Table 1 Trace elements composition and rare earth element (REE) (ppm) of Cambrian oncoids limestone from North China Platform

Element	WHXZ-1	WHXZ-2	WHXZ-3	DQZX-1	DQZX-2	DQZX-3
Li	1.022	1.463	0.887	0.925	1.063	1.151
Be	0.113	0.077	0.054	0.126	0.032	0.061
Sc	1.124	1.013	0.892	0.925	0.844	0.782
V	3.214	3.729	2.923	3.241	3.164	2.776
Cr	1.692	2.37	2.413	1.699	1.722	1.214
Co	1.911	0.767	1.032	1.228	1.453	1.393
Ni	8.231	7.629	8.654	8.618	8.146	7.88
Cu	2.926	2.943	2.868	2.447	2.571	2.415
Zn	8.547	8.262	9.301	9.469	8.897	7.324
Rb	0.171	0.114	0.152	0.139	0.14	0.143
Sr	124.022	149.87	131.073	132.135	131.674	132.383
Y	0.798	0.905	0.957	0.922	1.039	1.104
Zr	6.961	7.132	7.126	6.712	6.303	6.57
Nb	0.403	0.379	0.652	0.142	0.089	0.162
Mo	0.512	0.347	0.498	0.493	0.409	0.389
Sb	1.483	1.355	1.226	1.022	0.947	1.119
Ba	1.637	1.902	1.643	2.329	2.415	2.331
La	1.038	1.025	1.007	0.926	0.985	1.013
Ce	1.906	1.825	2.031	2.267	2.338	2.825
Pr	0.437	0.328	0.384	0.221	0.189	0.246
Nd	0.513	0.591	0.369	0.276	0.425	0.385
Sm	0.428	0.344	0.274	0.392	0.301	0.356
Eu	0.062	0.049	0.026	0.041	0.027	0.034
Gd	0.301	0.29	0.192	0.224	0.313	0.294
Tb	0.03	0.044	0.011	0.056	0.019	0.025
Dy	0.071	0.094	0.088	0.076	0.064	0.055
Ho	0.026	0.03	0.031	0.029	0.032	0.033
Er	0.063	0.051	0.036	0.049	0.048	0.054
Tm	0.016	0.019	0.013	0.018	0.012	0.017
Yb	0.127	0.124	0.118	0.078	0.065	0.082
Lu	0.0121	0.013	0.018	0.022	0.015	0.014
Hf	0.054	0.041	0.057	0.045	0.042	0.065
Ta	0.023	0.037	0.018	0.009	0.012	0.025
Pb	1.981	1.842	1.983	1.104	1.302	1.228
Th	0.394	0.458	0.411	0.392	0.385	0.407
U	0.211	0.314	0.238	0.252	0.199	0.241
V/Sc	2.86	3.68	3.28	3.50	3.75	3.55
V/Cr	1.90	1.57	1.21	1.91	1.84	2.29
Sr/Ba	75.76	78.80	79.78	56.73	54.52	56.79
Sr/Cu	42.39	50.92	45.70	53.99	51.21	54.82
V/V + Ni	0.28	0.33	0.25	0.27	0.28	0.26
Th/U	1.87	1.46	1.73	1.56	1.93	1.69
Cu/Zn	0.34	0.36	0.31	0.26	0.29	0.33
REE	7.69	7.52	7.31	6.48	6.77	7.39
LREE	4.38	4.16	4.09	4.12	4.27	4.86
HREE	1.44	1.57	1.46	1.47	1.61	1.68
LREE/HREE	3.04	2.65	2.79	2.79	2.65	2.89
$(La/Yb)_N$	0.77	0.78	0.80	1.12	1.43	1.17
$(La/Sm)_N$	2.43	2.98	3.68	2.36	3.27	2.85
$(Gd/Yb)_N$	1.41	1.39	0.97	1.71	2.87	2.14

Table 1 (continued)

Element	WHXZ-1	WHXZ-2	WHXZ-3	DQZX-1	DQZX-2	DQZX-3
Er/Nd	0.12	0.09	0.10	0.17	0.11	0.14
Y/Dy	11.24	9.63	10.88	12.13	16.23	20.07
Y/Ho	30.7	30.17	30.87	31.79	32.47	33.45
Ce/Ce*	0.51	0.64	0.61	1.17	1.41	1.32
Pr/Pr*	0.23	0.17	0.22	0.13	0.09	0.11
Eu/Eu*	0.60	0.57	0.39	0.45	0.34	0.38
Gd/Gd*	0.78	0.71	1.25	0.51	1.57	1.15
Element	XWDXZ-1	XWDXZ-2	XWDXZ-3	SDGZX-1	SDGZX-2	SDGZX-3
Li	0.826	0.772	0.964	0.688	0.721	0.736
Be	0.109	0.078	0.052	0.091	0.103	0.115
Sc	0.873	0.921	0.782	0.926	0.771	0.917
V	3.215	2.872	2.964	3.422	2.941	3.218
Cr	1.417	1.524	1.736	2.375	2.141	2.288
Co	1.13	0.889	0.925	0.747	1.028	0.857
Ni	7.282	7.648	8.125	9.361	9.243	8.736
Cu	2.523	2.631	2.422	2.492	2.545	2.381
Zn	8.225	9.374	7.209	9.062	8.452	8.209
Rb	0.151	0.143	0.168	0.117	0.122	0.105
Sr	123.01	121.101	128.645	113.002	120.801	117.925
Y	0.984	0.831	0.935	1.01	1.142	0.831
Zr	4.948	5.122	5.251	4.036	4.425	4.001
Nb	0.556	0.579	0.404	0.075	0.105	0.069
Mo	0.431	0.318	0.425	0.385	0.479	0.392
Sb	0.438	0.526	0.371	0.175	0.214	0.238
Ba	1.997	2.14	2.329	2.842	3.431	2.925
La	0.909	0.973	0.902	0.964	0.982	0.951
Ce	1.792	1.604	1.737	1.342	1.479	1.53
Pr	0.346	0.391	0.286	0.192	0.207	0.233
Nd	0.328	0.264	0.343	0.205	0.232	0.218
Sm	0.217	0.192	0.208	0.264	0.298	0.285
Eu	0.038	0.059	0.071	0.039	0.037	0.051
Gd	0.33	0.295	0.248	0.32	0.286	0.341
Tb	0.053	0.032	0.048	0.021	0.039	0.051
Dy	0.063	0.056	0.049	0.044	0.052	0.047
Ho	0.029	0.023	0.026	0.024	0.028	0.023
Er	0.062	0.053	0.064	0.042	0.049	0.051
Tm	0.018	0.014	0.012	0.023	0.011	0.011
Yb	0.133	0.142	0.11	0.081	0.073	0.095
Lu	0.019	0.018	0.017	0.024	0.018	0.013
Hf	0.059	0.042	0.058	0.031	0.033	0.029
Ta	0.017	0.029	0.016	0.013	0.011	0.012
Pb	1.617	1.536	1.429	1.632	1.307	1.453
Th	0.548	0.419	0.371	0.397	0.374	0.382
U	0.302	0.259	0.361	0.202	0.194	0.236
V/Sc	3.68	3.12	3.79	3.70	3.81	3.51
V/Cr	2.27	1.88	1.71	1.44	1.37	1.41
Sr/Ba	61.60	56.59	55.24	39.76	35.21	40.32
Sr/Cu	48.76	46.03	53.12	45.35	47.47	49.53
V/V + Ni	0.31	0.27	0.27	0.27	0.24	0.27

Table 1 (continued)

Element	XWDXZ-1	XWDXZ-2	XWDXZ-3	SDGZX-1	SDGZX-2	SDGZX-3
Th/U	1.81	1.62	1.03	1.97	1.93	1.62
Cu/Zn	0.31	0.28	0.34	0.27	0.30	0.29
REE	6.88	6.40	6.36	5.86	5.71	6.01
LREE	3.63	3.48	3.55	3.01	3.24	3.27
HREE	1.69	1.46	1.51	1.59	1.70	1.46
LREE/HREE	2.15	2.38	2.35	1.89	1.91	2.23
$(La/Yb)_N$	0.64	0.65	0.77	1.12	1.27	0.94
$(La/Sm)_N$	4.19	5.07	4.34	3.65	3.30	3.34
$(Gd/Yb)_N$	1.48	1.24	1.34	2.36	2.34	2.14
Er/Nd	0.19	0.20	0.19	0.20	0.21	0.23
Y/Dy	15.62	14.84	19.082	22.95	21.961	17.68
Y/Ho	33.93	36.13	35.96	42.08	40.79	36.13
Ce/Ce*	0.60	0.48	0.70	0.80	0.82	0.75
Pr/Pr*	0.22	0.29	0.18	0.18	0.17	0.19
Eu/Eu*	0.59	1.03	1.24	0.54	0.48	0.65
Gd/Gd*	0.79	0.77	0.48	1.26	0.84	0.75

All concentrations are in ppm

oxygen-enriched environment [46], and $V/(V+Ni) < 0.6$ denotes the oxidizing environment [47]. The value of V/Sc is 2.86 to 3.81 in oncoids indicating weak V enrichment [45]. Likewise, V/Cr of oncoids averages 1.73 and V/(V + Ni) ratio ranges from 0.24 to 0.33, which suggests that the marine carbonate oncoids of the North China Platform were developed in an oxic environment (Table 1).

The trace element contents of carbonates and their ratios, particularly Sr/Ba and Sr/Cu, are important proxies for paleosalinity and paleoclimate of the sedimentary environment [48]. If Sr/Ba is > 1, it is indicative of marine environment, whereas $Sr/Ba < 1$ is suggestive of terrestrial deposit [49]. The regional Sr/Ba values of oncoids averaged 57.59, with a small variation range (35.21–79.78), representing typical marine deposition and reflecting the characteristics of high salinity of early Cambrian seawater on the North China Platform. Furthermore, the range of Sr/Cu value (1.3 to 5.0) indicates humid climate, while the value greater than 5.0 shows arid climate [50]. The Sr/Cu value of the oncolitic samples ranges from 42.39 to 54.82, with an average of 49.11, suggesting arid climatic conditions (Table 1).

Fe_2O_3/FeO has been used to delineate oxygen fugacity in depositional settings. However, this ratio is prone to changes by later geological processes and, thus, difficult to be used as a proxy for the redox conditions of original sedimentary paleoenvironment [51]. Instead, the values of Cu/Zn together with Th/U can be indicative to the redox conditions of marine environment [52]. Previous studies demonstrated that if the value of Cu/Zn is less than 0.21, it implies reducing environment, whereas a range value of 0.21–0.35 suggests hypoxia and 0.35–0.50 oxic [51, 53]. On the other hand, if Th/U ratio is less than 2, it exhibits the marine environment [54]. The results of the present study display Cu/Zn ranges from 0.26 to 0.36 and Th/U ratios 1.02–1.97 which implies that oncoids of the North China Platform developed in a hypoxic marine environment.

4.2.2 Rare Earth Elements

Rare earth elements in carbonate rocks are principally inherited from ancient seawater. However, in most cases, the contents of rare earth elements in ancient carbonates were also influenced by terrigenous clastic input in addition to diagenesis. Therefore, rare earth elements of oncoids can reflect the external and endogenic environmental conditions [55].

ΣREE of oncolitic samples from the North China Platform reveals that the mean value is 6.70×10^{-6} and ranges from 5.71×10^{-6} to 7.69×10^{-6}, which is much lower than NASC 173.2×10^{-6} [56] and in accordance with the characteristics of ΣREE in carbonate rocks being lower than 100×10^{-6} [57]. Moreover, the LREE/HREE of these samples ranges from 1.89 to 3.04 with a mean value of 2.48 that is lower than NASC, 6.95, and denotes the weak enrichment characteristics of light rare earth elements. Besides, $(La/Yb)_N$, $(La/Sm)_N$ and $(Gd/Yb)_N$ signify slope of distribution curve of rare earth elements, normalized by NASC [58], and also define enrichment degree. $(La/Yb)_N$ and $(La/Sm)_N$ reflect the fractionation degree of LREEs; however, $(Gd/Yb)_N$ exhibits the fractionation degree of HREEs [59, 60]. The $(La/Yb)_N$ and $(La/Sm)_N$ values of oncoid samples from the North China Platform show that $(La/Yb)_N$ ranges from 0.64 to 1.43 and $(La/Sm)_N$ ranges from 2.36 to 5.07,

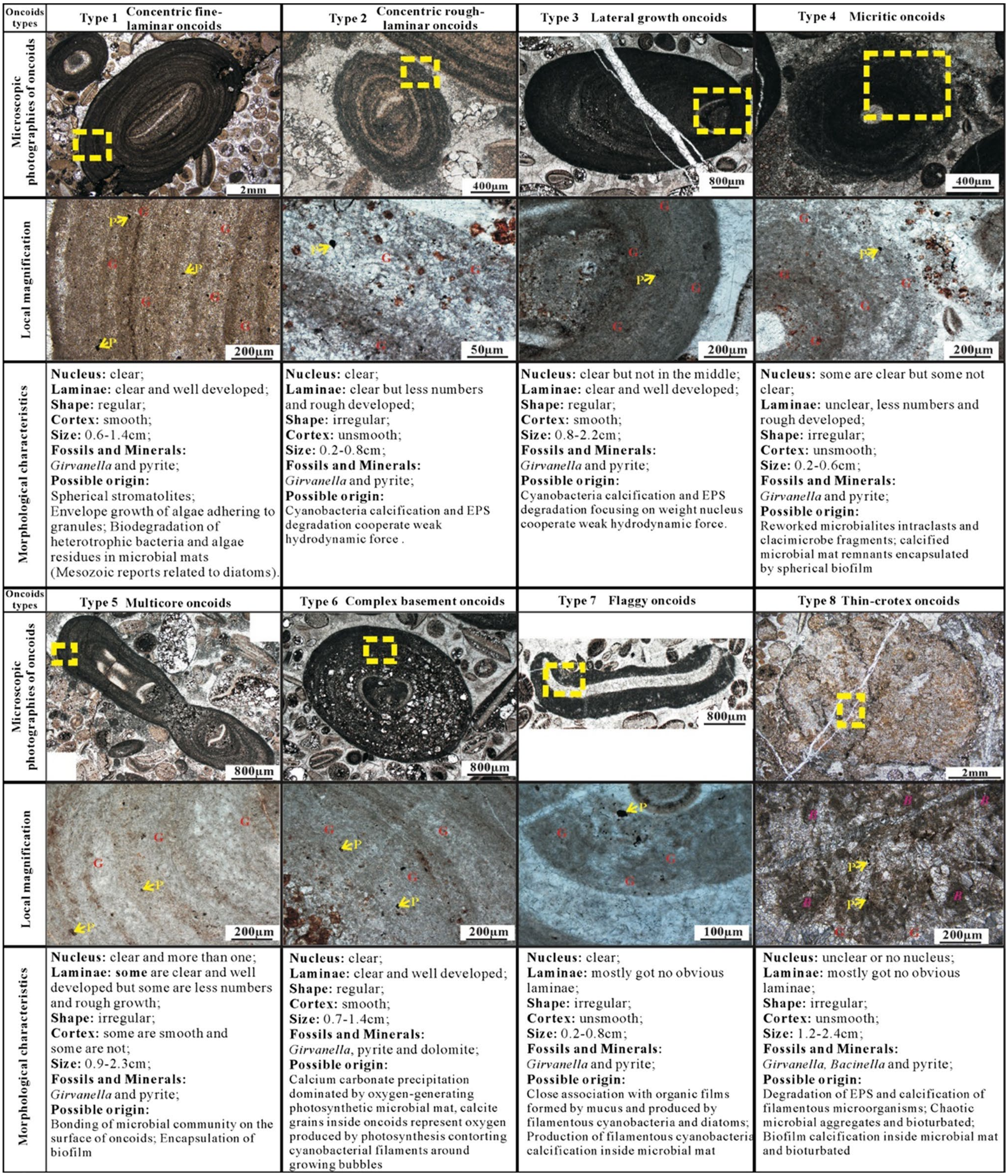

Fig. 4 Morphological classifications of oncoids from the Cambrian Miaolingian Series strata in North China Platform. The basic morphological characteristics of different types of oncoids, occurrences of microbial fossils and pyrite particles

which suggests that the fractionation degree of light rare earth elements in the study area is low. The $(Gd/Yb)_N$ of the Cambrian oncolitic samples ranges from 0.97 to 2.87, demonstrating that the heavy rare earth elements in study area are more augmented.

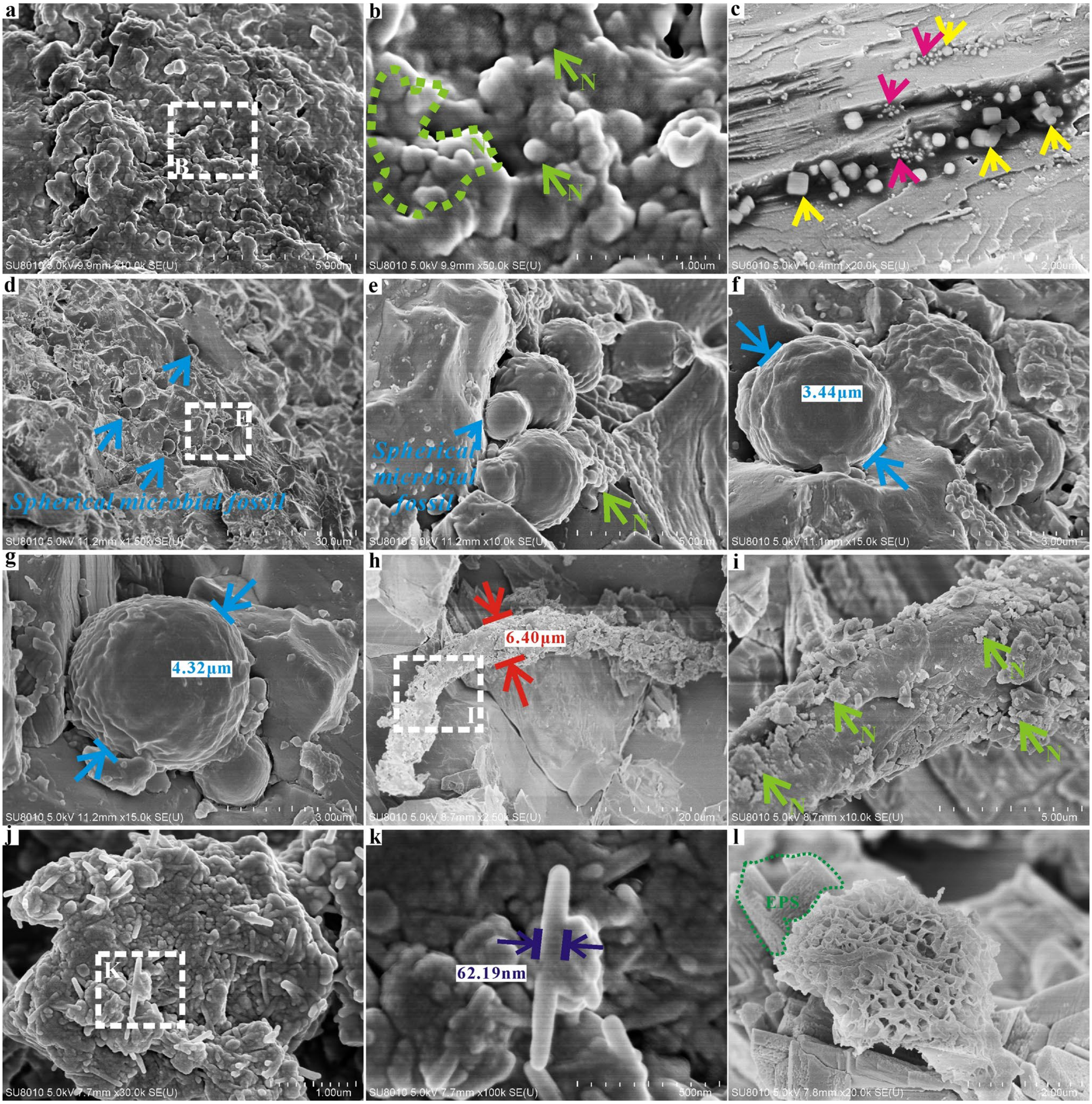

Fig. 5 Ultramicro-fabric of micrite inside oncoids from Cambrian Miaolingian Series strata. **a** The main structure of dark micrite, amorphous calcium carbonate mineral carbonate mud; **b** the local magnification of **a**, green arrows show nanospheres, and area reveals the community of nanospheres, N-nanospheres; **c** two kinds of pyrite particles observed inside micrite, yellow arrows indicate framboidal pyrite, pink arrows exhibit normal pyrite grains; **d** spherical calcified microorganism fossils (blue arrows) inside dark micrite; **f** the local magnification of **a** shows the nanospheres (blue arrow) growth around spherical calcified microorganism fossils; **f** and **g** depict the diameter of spherical calcified microorganism fossils; **h** filamentous microbial fossils inside dark micrite; **i** the local magnification of **h** shows that the nanospheres (green arrow) grow on the surface of filamentous microbial fossil; **j** rod-like microbial fossils community inside dark micrite; **k** the local magnification of **j** indicates the diameter of rod-like microbial fossil; **l** echinoderm debris or honeycomb-like microbial fossils, calcification EPS

Y, Dy, Ho, Er and Nd in carbonate rocks are effective indicators to distinguish the marine and non-marine sedimentary environments [51, 61–63]. The Y/Ho ratio of modern seawater ranges from 44 to 74 [64], and that of normal limestone is around 44 [65]. The average Y/Ho ratio of oncolitic samples is 34.54, which is similar to the values

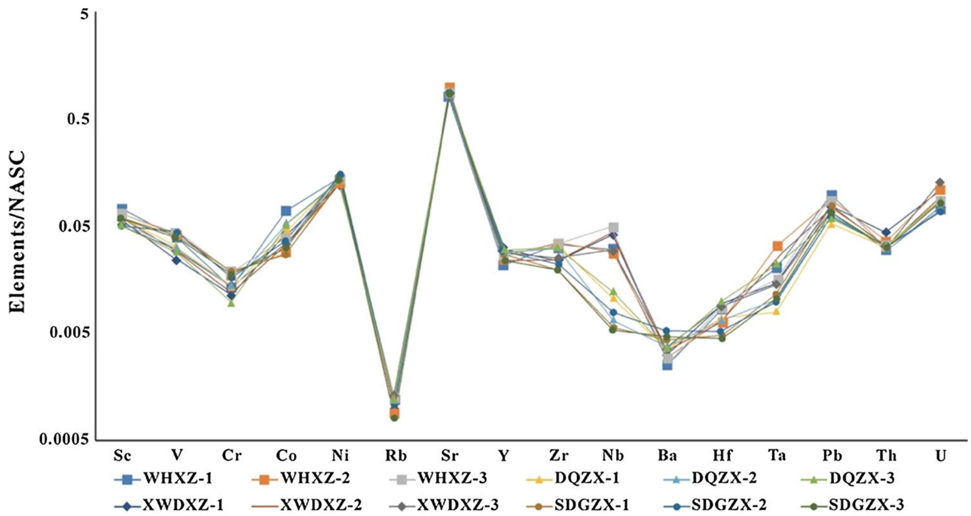

Fig. 6 NASC-normalized trace elements patterns of oncolitic samples from Cambrian Miaolingian Series, North China Platform

preserved by the normal limestone and higher than that of NASC (25.96; [58]). These ratios signify that the formation of oncoids was evidently influenced by terrigenous clasts [66]. Moreover, Y and Ho have close ionic radius and represent consistent geochemical behavior in geological environment [67]. Y/Ho in minerals or siliceous clastic rocks typically remains constant (27), for instance, the average value of North American shale and post-Archaean shale [68]. In addition, Y/Ho values in freshwater are very close to the average values of post-Archaean shales, but higher in seawater. The Y/Ho ratio in limestone is commonly around 44 [65], much higher than the terrigenous rocks. This ratio also conflicts with the ratio in marine carbonate sediments. For example, the Y/Ho ratio in the South Pacific Ocean is about 57 [64], while the Coral Sea in the West Pacific Ocean has Y/Ho as high as almost 80 [69]. Therefore, Y/Ho ratio has been often used as a marker for documentation of marine and continental sediments. The Y/Ho and Y/Dy ratios of oncoid samples from the North China Platform exhibit good linear relationship with correlation coefficient 0.7672 (Fig. 8), reflecting characteristics of rare earth elements in ancient seawater.

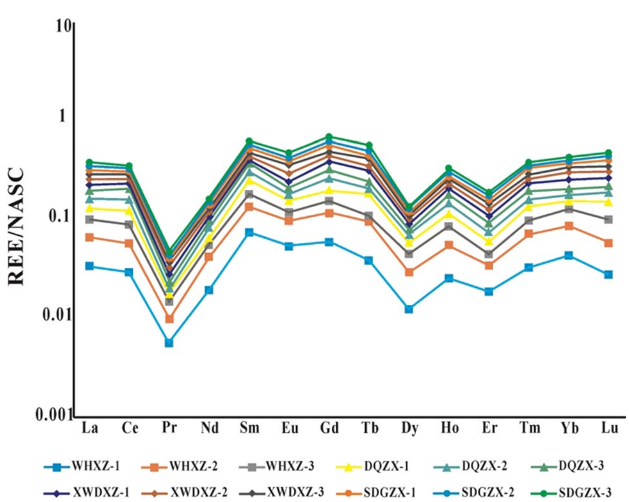

Fig. 7 NASC-normalized REE patterns of oncolitic samples from Cambrian Miaolingian Series, North China Platform

On the other hand, content of Zr in terrigenous clastic rocks is relatively high. When influenced by terrigenous materials, marine limestone is often characterized by enrichment zircon with good correlation between Zr and ΣREE [70]. Results of oncolitic samples depict a positive correlation, demonstrating that the rare earth elements in the samples are contaminated by terrestrial sources (Fig. 7). Besides this, Er/Nd values in normal seawater are about 0.27, which may decrease even lower than 0.1 under contamination of terrestrial materials or diagenesis [71]. The Er/Nd ratios of the Cambrian oncolitic samples range from 0.09 to 0.23 (mean value is 0.16), indicating the influx of terrestrial materials.

In diverse diagenetic environments, Eu and Ce can change their valence states and display anomalies, therefore providing invaluable information on diagenetic environment [72]. Ce has valence states of +3 and +4, and Ce^{3+} is simply oxidized to Ce^{4+} in marine environment and hydrolyzed, which is adsorbed and precipitated by iron and manganese oxide colloids. Under reduction conditions, oxides, for instance iron and manganese, dissolve, and Ce^{4+} is reduced to Ce^{3+} and the relative enrichment of Ce may occur locally [72]. Therefore, Ce anomalies (Ce/Ce*) of carbonate rocks can be effectively used to discriminate the change of redox conditions in paleo-ocean. It was proposed that when $Ce/Ce^* < 1$, Ce is relatively deficient and signifies oxidation condition; however, $Ce/Ce^* \approx 1$ represents neither enrichment nor depletion and exhibits reducing conditions. If $Ce/Ce^* > 1$, it suggests enrichment of Ce and shows oxidation conditions [73–75]. The variation range of Ce/Ce* of Cambrian oncoid samples is 0.48–1.41, with an average value of 0.82.

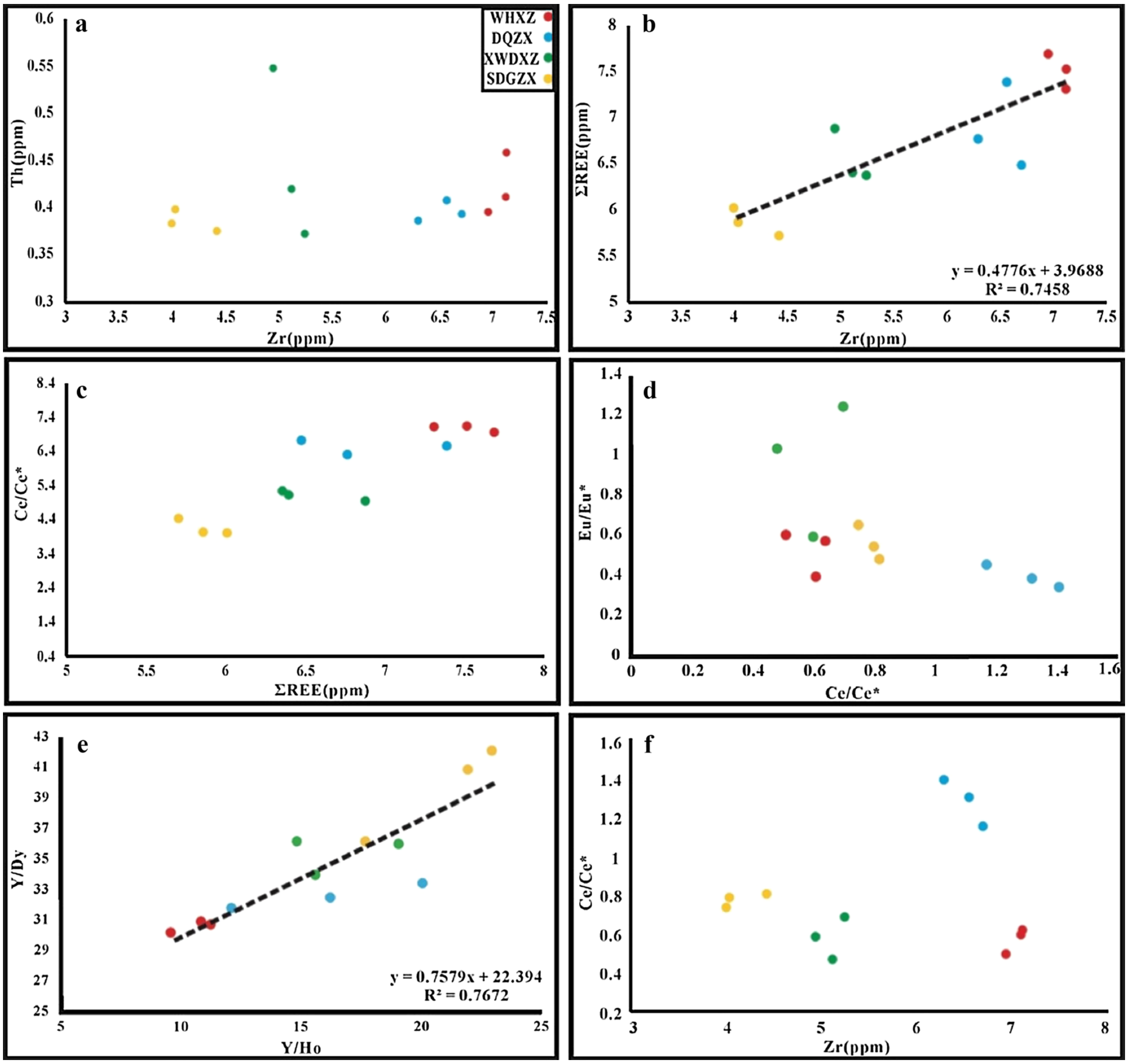

Fig. 8 **a** Zr–Th, **b** ΣREE–Zr, **c** ΣREE–Ce/Ce*, **d** Ce/Ce*–Eu/Eu*, **e** Y/Ho–Y/Dy, **f** Zr–Ce/Ce* of oncolitic limestone from Cambrian Miaolingian Series, North China Platform

Shields and Stlle [59] pointed out that diagenesis can change Ce anomaly values, which leads to a good correlation between Ce and Eu and REE. The relationship between Ce/Ce*, Eu/Eu* and REE of carbonate samples in the study area is presented in Fig. 8. There is no obvious correlation between these parameters, which suggests that the influence of diagenesis on oncoids of study area is limited. Moreover, Eu has two valence states including Eu^{2+} and Eu^{3+} in modern seawater. In strong acidic reducing environment, Eu is reduced to Eu^{2+} which differentiates it from adjacent elements, making it easier for Eu^{2+} to replace Eu into carbonate lattice and produce positive anomaly of Eu [60]. In the study area, the Eu/Eu* of oncoid samples is 0.34–1.03, with an average of 0.60, which represents no positive abnormality [76–79]. Besides this, the Gd/Gd* ratios of oncolitic samples range from 0.48 to 1.57 (average value is 0.90) and indicate slight negative anomalies, close to the modern seawater [65].

5 Discussion

5.1 Cambrian Oncoids Origin and Environment of Formation

5.1.1 Origin of Oncoids

In this study, the oncoids reveal considerable morphological differences and can be therefore classified into several groups (Fig. 4). Nevertheless, some similarities were noticed in the microscopic structure of these oncoids, specifically emergence of large number of *Girvanella* fossils and pyrite grains (Fig. 4). Based on these evidences, it is reasonable to suggest that the formation of oncoids in study area was closely associated with the participation of microorganisms [2, 6, 7, 12, 15–17, 19, 80, 81]. Moreover, in some well-developed oncoids with regular morphology, the directional arrangements of *Girvanella* fossils contain parallel bright and dark laminae, implying that these oncoids are formed by cyanobacteria-dominated calcification [40–42]. In addition, a large number of pyrite particles were found in the oncoids, pointing out toward the contribution of sulfate-reducing bacteria [43, 82–84] in the degradation of organic matter during the formation of oncoids. These features evidently suggest that the oncoids of the present study are associated with microorganisms. The origin of these oncoids is believed to be related to the productions of cyanobacteria-dominated microbial mats calcification and the degradation by heterotrophic bacteria (pyrite particles produced by sulfate reduction reaction dominated by SRB—sulfate-reducing bacteria) [43].

5.1.2 Environmental Conditions for Oncoid Formation

The global ocean evolved into an oxidizing environment from 1000 to 540 Ma and remained in oxidizing state to present, although several intermittent global anoxic events took place [85–87]. Elemental cycling between seawater and sediments is influenced by redox conditions, and the solubility of variable valence elements such as Mn, Mo, Cr, V and U varies greatly with the change of redox conditions, which leads to the elemental differentiation in sediments. For example, Ni, Co, Cu and Zn promote sulfide precipitation under reductive conditions, which leads to the corresponding depletion or enrichment of elements in sediments [88, 89]. Therefore, the geochemical behaviors of these elements are sensitive indicators for the change of redox conditions in the paleo-ocean. Table 1, Figs. 8 and 9 show that: (1) V/Cr ratio of oncoids averages in 1.73, which is lower than 2 [46]; (2) V/Sc ratio ranges from 2.86 to 3.81 and averages in 2.53 indicating V enrichment relative to Sc [45]; (3) V/(V + Ni) ranges from 0.24 to 0.33, which is lower than 0.6 [47]; (4) Cu/Zn ranges from 0.26 to 0.36, averages in 0.31, which is higher than 0.21 [51, 53]. Based on these findings and abundance of pyrite inside oncoids, it is confirmed that the oncoids formed in oxidizing environment.

Paleosalinity is an important indicator for examining the characteristics of geological and historical sedimentary environment. In natural waters, Sr is stronger than Ba in migration capability. When salinity of water medium is very low, Sr and Ba appear in the form of bicarbonate. Additionally, when salinity of environment increases gradually, Ba precipitates prior in the form of $BaSO_4$, which makes Sr/Ba ratios tend to augment. Likewise, salinity of water body increases to a certain extent, and Sr also precipitates in the form of $SrSO_4$. Therefore, Sr abundance and Sr/Ba ratio recorded in sediments are positively correlated with paleosalinity. It is commonly reflected that if Sr/Ba > 1, it is indicative of marine deposit and Sr/Ba < 1 is suggestive of continental deposit, and the greater the values, the higher will be the salinity [90]. Besides this, Sr/Cu is also important to indicate the drought and humidity of paleoenvironment [50]. The result of these oncolitic samples reveals that: (1) Sr/Ba in the study area ranges from 39.76 to 79.78 (mean value = 57.59) which is higher than 1; (2) Sr/Cu value ranges from 42.39 to 54.82, with an average of 49.11; (3) Th/U ranges from 1.03 to 1.97 (mean value = 1.68). These findings suggest that these oncoids, which developed in shallow marine environment, are affected by higher paleosalinity and drought.

5.1.3 Influences of Terrestrial Factors and Diagenesis

The characteristics of elements in sediments are primarily governed by provenance; however, carbonate rocks are the products of endogenous sedimentation, and their elements are generally inherited from paleoseawater, but can be susceptible to terrestrial minerals and late diagenesis [59]. Therefore, trace and rare earth elemental analysis of

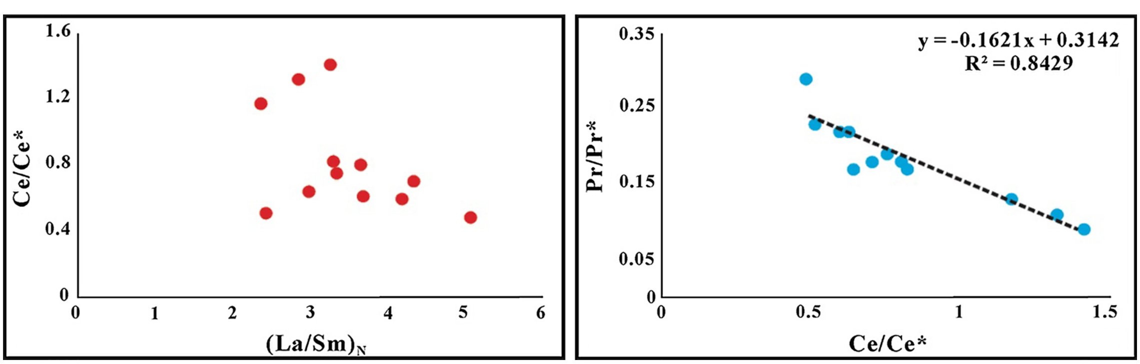

Fig. 9 $(La/Sm)_N$–Ce/Ce* and Ce/Ce*–Pr/Pr* of oncolitic limestone from Cambrian Miaolingian Series, North China Platform

carbonate rocks can reflect their environment of formation, terrestrial weathering processes and diagenesis influenced [51]. Zr, Th, Er/Nd and Y/Ho are important to understand the terrestrial influence [61–63, 66, 78]. The results of trace elements and REEs analysis of these oncolitic samples reveal that: (1) average of Y/Ho is 34.5 which is lower than the normal carbonate rocks, i.e., 44 [65]; (2) Zr and Th occur with an average of 5.72 ppm and 0.41 ppm, and in obvious correlation in Fig. 7; (3) Zr has good linear correlation with rare earth elements (Fig. 7); (4) average of Er/Nd is 0.16 which is lower than normal marine environment (i.e., 0.27) [71]; (5) moreover, Pr/Pr* is calculated as lower than 1. These results evidently show that the formation processes of oncoids experienced terrestrial influences.

Moreover, the results of Ce/Ce*, Eu/Eu*, $(La/Yb)_N$ and $(La/Sm)_N$ signify that: (1) no significant correlation is found between Ce/Ce* with Eu/Eu* (Fig. 7); (2) no correlation is observed between Ce/Ce* with ΣREE (Fig. 7); (3) average of $(La/Sm)_N$ is 3.45, which is more than 1 and indicates no obvious correlation with Ce/Ce* (Fig. 9); (4) Ce/Ce* ratio portrays obvious correlation with Pr/Pr* with correlation coefficient 0.8429 (Fig. 9). These results strongly support the idea that LREEs from oncolitic samples were principally inherited from paleomarine environment, whereas HREEs predominantly were derived from land-based factors, and the formation processes are less affected by diagenesis.

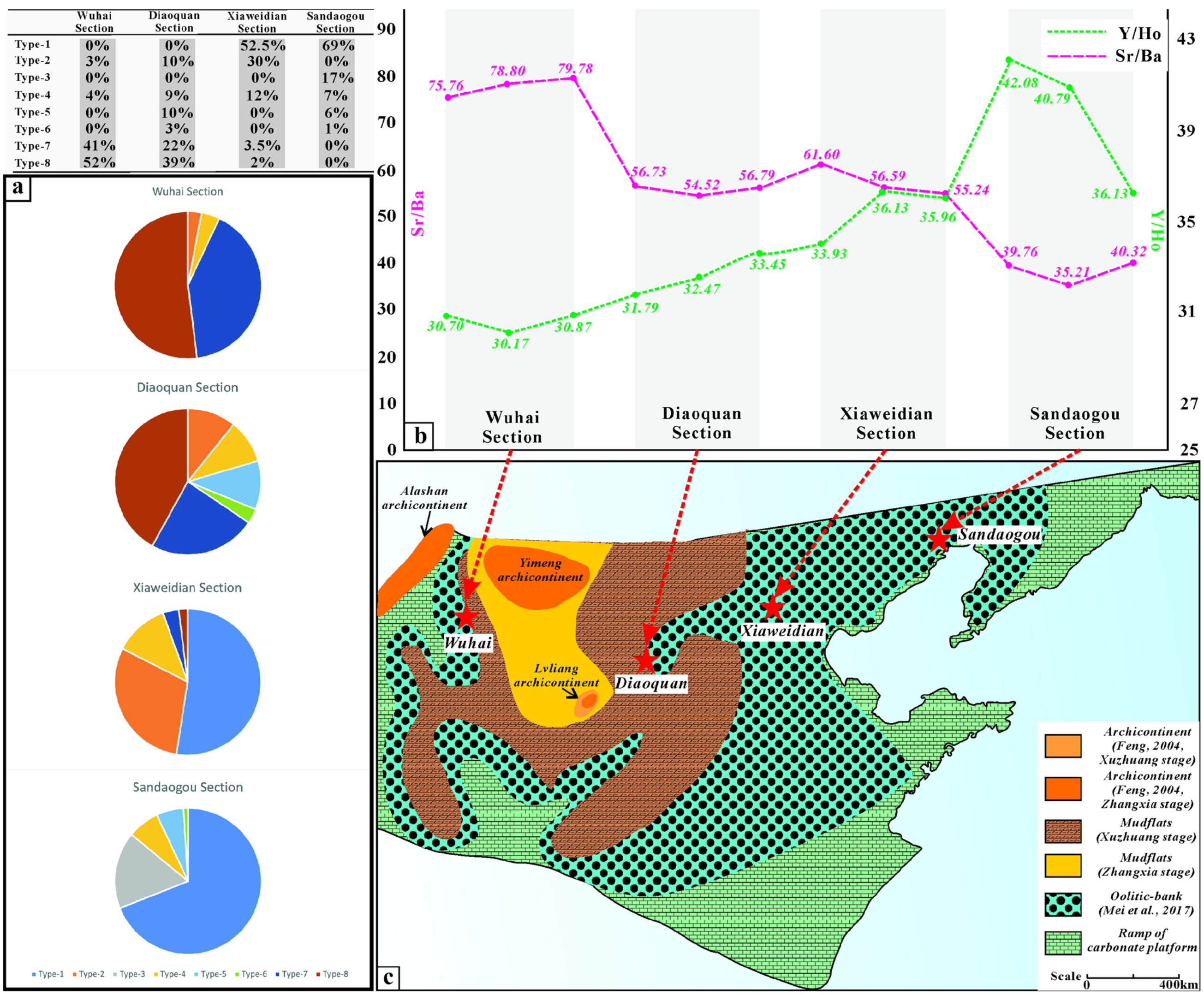

	Wuhai Section	Diaoquan Section	Xiaweidian Section	Sandaogou Section
Type-1	0%	0%	52.5%	69%
Type-2	3%	10%	30%	0%
Type-3	0%	0%	0%	17%
Type-4	4%	9%	12%	7%
Type-5	0%	10%	0%	6%
Type-6	0%	3%	0%	1%
Type-7	41%	22%	3.5%	0%
Type-8	52%	39%	2%	0%

Fig. 10 **a** The types and proportions of different oncoids in each section as observed under microscope, 200 randomly selected samples of oncoids from each section. According to the classification of morphological characteristics (part 4.2), the proportions of each type of oncoids in different sections are counted; **b** variation trend of Y/Ho and Sr/Ba of four sections; **c** the paleogeographic location of the four sections reported in this study and the division of paleogeographic facies zones are modified from Feng [29] and Ma et al. [91]

5.2 Effects of Paleogeographic Factors on Oncoid Morphology

The Miaolingian oncoids from four different sections in the North China Platform (Fig. 1) are classified according to morphology by investigating their petrographic characteristics (Fig. 4). The results depict that the morphologically different oncoids are distributed non-proportionally among various sections. Two hundred individual oncoid samples were randomly selected from each section and were statistically analyzed for different oncoid populations (Fig. 10a).

The statistical results reveal that the fraction of oncoid species in the four sections illustrates an obvious polarization trend. Type 7 and Type 8 oncoids represent 93% and 61% of total oncoids population in the Wuhai and Diaoquan sections (the western sections), respectively. However, the Type 1 oncoids indicate a fraction of 52.5% and 69% in Xiawidian and Sandaogou sections (the eastern sections), respectively (Fig. 10a). Based on the morphological classification of these oncoids (Fig. 4), the more regular and exquisitely developed oncoids are expected to be found in the eastern sections (Xiaweidian and Sandaogou sections), while the rough, irregular and uneven oncoids are more likely found in the two sections toward the west (Wuhai and Diaoquan sections) (Fig. 10b).

The geochemical data from different sections of oncolitic samples were examined to explain the morphological differentiation of oncoids in regional correlation. Y/Ho reflects the impact of terrigenous debris on sedimentary environment [65], while Sr/Ba reflects the salinity of marine environment during the formation of the oncoids [90]. The variation trend of Y/Ho and Sr/Ba indicates that the paleosalinity and terrigenous influences are higher in the western sections and lower in the eastern sections. This variation trend can be explained in terms of paleogeographic location. In the Miaolingian epoch, the Yimeng and Lvliang regions were located in the western part of the North China Platform (Fig. 10c), while Wuhai and Diaoquan sections were closer to paleocontinent. Shorter distance between the sedimentary areas and the paleocontinent led to an increased salinity in the paleo-oceanic environment. Moreover, the difference in paleogeographic location led to the varying influence of land-derived factors on the formation of oncoids. Additionally, the microbial mat sedimentation dominated by cyanobacteria might be fully influential, where the marine environment having more suitable salinity in offshore was less influenced from terrigenous debris, resulting in regular shape and development of oncoids in addition to well-developed laminae. On the other hand, in the nearshore areas with higher salinity and more terrigenous debris impact, oncoids have irregular shape with poor lamina development.

6 Conclusions

1. A large number of filamentous microbial fossils have been documented in the Miaolingian carbonate oncoids from the Wuhai, Diaoquan, Xiawidian and Sandaogou sections along the North China Platform. The morphological characteristics of these fossils typically resemble the filamentous cyanobacteria fossils *Girvanella*. From the SEM observations of the oncoid microstructure and the framboidal pyrite particles observed in the oncoids, a microbial carbonate is concluded for the marine oncoids from the North China Platform.
2. Geochemical analysis of these oncoids shows the presence of rare earth and trace elements. The geochemical statistical measurements indicate that these oncoids were formed in a lagoonal setting and were affected by oxidation, evaporative drought, higher salinity and terrigenous debris.
3. The ratios of Y/Ho and Sr/Ba are interpreted to know the morphological differences among these shallow marine sediments and the influence of paleogeographic factors on their morphological characteristics. Influence of terrigenous debris increases near the continent, i.e., Wuhai and Diaoquan sections, characterized by high paleosalinity that results in irregular growth of oncoids with poor development of laminae and non-smooth cortexes. In contrast, the terrigenous debris was less influential when the sedimentary area was away from the continent, i.e., Xiaweidian and Sandaogou sections. Likewise, lower paleosalinity resulted in regular morphology of the oncoids developing perfect laminae and smooth cortexes.

Acknowledgements We gratefully acknowledge Prof. Mingxiang Mei, Prof. Yinhui Zuo and Dr. Yangbo Lu for the critical reviews on the earlier version of the manuscript. We are also thankful for the generous financial support from the National Natural Science Foundation of China (Grant Nos. 41472090, 40472065) and the timely help from Liying Zhao, Xinjing Li and Hang Jiao of Research Institute of Petroleum Exploration and Development, CNPC.

References

1. Heim, A.: Monographie der Churfirsten-Mattstock-Gruppe. 3. Teil: Stratigraphie der Unteren Kreide und des Jura. Zur Lithogenesis. Beitr. geol. Karte Schweiz. **20**, 369–662 (1916)
2. Flugel, E.: Microfacies of Carbonate Rocks, pp. 128–129. Springer, Heidelberg (2010)
3. Jones, B.; Renaut, R.W.: Formation of silica oncoids around geysers and hot springs at El Tatio, Chile. Sedimentology **44**(2), 287–304 (1997)
4. Hägele, D.; Leinfelder, R.; Grau, J.; Burmeister, E.-G.; Struck, U.: Oncoids from the river Alz (southern Germany): tiny ecosystems in a phosphorus-limited environment. Palaeogeogr. Palaeoclim. **237**(2–4), 378–395 (2006)

5. Shapiro, R.S.; Fricke, H.C.; Fox, K.: Dinosaur-bearing oncoids from ephemeral lakes of the Lower Cretaceous Cedar Mountain Formation, Utah. Palaios **24**(1), 51–58 (2009)
6. Han, Z.; Zhang, X.; Chi, N.; Han, M.; Woo, J.; Lee, H.S.; Chen, J.: Cambrian oncoids and other microbial-related grains on the North China Platform. Carbonate Evaporites **30**(4), 373–386 (2015)
7. Wang, H.; Xiao, E.Z.: Oncolites in Cambrian Series 3 at Diaoquan section in Lingqiu. Shanxi J. Northeast Pet. Univ. **42**(5), 44–53 (2018). **(in Chinese with English abstract)**
8. Tucker, M.E.; Wright, V.P.: Carbonate Sedimentology, pp. 1–482. Wiley-Blackwell, Oxford (1990)
9. Li, X.Z.; Guan, S.R.; Xie, Q.B.; Wang, Z.: The oncoids genesis in the Middle Member of the Guanzhuang Formation of Eocene in Pingyi Basin. Acta Pet. Sin. **16**(2), 261–268 (2000). **(in Chinese with English abstract)**
10. Schaefer, M.O.; Gutzmer, J.; Beukes, N.J.: Late Paleoproterozoic Mn-rich oncoids: earliest evidence for microbially mediated Mn precipitation. Geology **29**(9), 835–838 (2001)
11. Shi, G.R.; Chen, Z.Q.: Lower Permian oncoids from South China: implications for equatorial sea-level responses to Late Paleozoic Gondwanan glaciation. J. Asian Earth Sci. **26**(3–4), 424–436 (2006)
12. Reolid, M.; Nieto, L.M.: Jurassic Fe–Mn macro-oncoids from pelagic swells of the External Subbetic (Spain): evidences of microbial origin. Geol. Acta **8**(2), 151–168 (2010)
13. Olivier, N.; Cédric, C.; Martin-Garin, B.; Lathuilière, B.; Gaillard, C.; Ferry, S.; Hantzpergue, P.; Geister, J.: Coral-microbialite reefs in pure carbonate versus mixed carbonate–siliciclastic depositional environments: the example of the Pagny-sur-Meuse section (Upper Jurassic, northeastern France). Facies **50**(2), 229–255 (2004)
14. Brigaud, B.; Durlet, C.; Deconinck, J.F.; Vincent, B.; Puceat, E.; Thierry, J.; Trouiller, A.: Facies and climate/environmental changes recorded on a carbonate ramp: a sedimentological and geochemical approach on Middle Jurassic carbonates (Paris Basin, France). Sediment. Geol. **222**(3), 181–206 (2009)
15. Yang, R.; Fan, A.; Han, Z.Z.; Chi, N.J.: Status and prospect of studies on oncoid. Adv. Earth Sci. **26**(5), 465–474 (2011). **(in Chinese with English abstract)**
16. Zhang, W.H.; Shi, X.Y.; Tang, D.J.; Jiang, G.Q.: Oncoids from lower-middle Cambrian transition of the western north china platform: a study of their ultra-fabrics and biomineralization. Geoscience **28**(1), 1–15 (2014). **(in Chinese with English abstract)**
17. Zhang, W.H.; Shi, X.Y.; Tang, D.J.; Wang, X.: Mass-occurrence of oncoids in the early-middle Cambrian transition at western margin of north china platform: a response of microbial community to shallow marine anoxia. J. Palaeogeogr. **16**(3), 305–318 (2014). **(in Chinese with English abstract)**
18. Zhou, G.; Zheng, R.; Zhao, G.: Characteristics, origin and geological significance of Oncoids of Givetian (Middle Devonian) in Ganxi Area, Northwestern Sichuan. J. Jilin Univ. **47**(2), 405–417 (2017). **(in Chinese with English abstract)**
19. Mei, M.X.; Riaz, M.; Liu, L.; Meng, Q.F.: Oncoids built by photosynthetic biofilms: an example from the Series 2 of Cambrian in the Liaotung Peninsula. J. Palaeogeogr. **21**(1), 31–48 (2019). **(in Chinese with English abstract)**
20. Védrine, S.; André, S.; Hug, W.: Oncoid growth and distribution controlled by sea-level fluctuations and climate (Late Oxfordian, Swiss Jura Mountains). Facies **53**(4), 535–552 (2007)
21. Védrine, S.: Co-occurrence of the foraminifer *Mohlerina basiliensis* with Bacinella–Lithocodium oncoids: palaeoenvironmental and palaeoecological implications (Late Oxfordian, Swiss Jura). J. Micropalaeontol. **27**(1), 35–44 (2008)
22. Zhang, Y.Y.; Jun, Y.H.; Po, W.J.; Korla, G.: Oncolites from the Lianglitag Formation (Kaitian, Upper Ordovician), Tazhong, Tarim Block, NW China. Acta Micropalaeontol. Sin. **26**(3), 234–242 (2009). **(in Chinese with English abstract)**
23. Peryt, T.M.: Classification of coated grains. In: Peryt, T.M. (ed.) Coated Grains. Springer, Berlin (1983)
24. Zhang, K.M.; Huang, W.H.; Wang, J.H.: Characteristics and environmental significance of Lacustrine Oncolites in Paleogene Guanzhuang Formation in Pingyi Basin, Shandong Province in Eastern China. Acta Sediment. Sin. **31**(2), 259–268 (2013). **(in Chinese with English abstract)**
25. Zhang, X.Y.; Qi, Y.A.; Dai, M.; Chai, S.: Coupling variation of oncoids and trace fossils in the Zhangxia Formation (Cambrian Miaolingian Series), Dengfeng, western Henan Province. Acta Micropalaeontol. Sin. **32**(2), 184–193 (2015). **(in Chinese with English abstract)**
26. Dai, M.Y.; Qi, Y.A.; Chang, Y.G.; Wang, M.; Li, D.: Oncoids and their significance from the Second Member of the Mantou Formation (Cambrian Series 3), Dengfeng Area, Henan. Acta Sediment. Sin. **32**(3), 410–417 (2014)
27. Qi, Y.A.; Chai, S.; Zhang, X.Y.; Dai, M.Y.; Wang, M.: Oncoids and their depositional features from the second member of Mantou Formation (Cambrian Series 3), Weihui area, Henan Province. China Sci. Pap. **21**(11), 2416–2421 (2016). **(in Chinese with English abstract)**
28. Meng, X.H.; Ge, M.; Tucker, M.E.: Sequence Sequence stratigraphy, sea-level changes and depositional systems in the Cambro-Ordovician of the North China carbonate platform. Sediment Geol. **114**(1), 189–222 (1997)
29. Feng, Z.Z.; Peng, Y.M.; Jin, Z.K.; Bao, Z.D.: Lithofacies paleogeography of the Cambrian and Ordovician in China, pp. 112–121. Petroleum Industry Press, Beijing (2004). **(In Chinese)**
30. Wang, H.Z.; Shi, X.Y.; Wang, X.L.; Yin, H.F.; Qiao, X.F.: Research on the Sequence Stratigraphy of China, pp. 1–457. Guangdong Science and Technology Press, Guangzhou (2000). **(in Chinese)**
31. Haq, B.U.; Schutter, S.R.: A chronology of Paleozoic sea-level changes. Science **322**(5898), 64 (2008)
32. Peng, S.; Babcock, L.; Cooper, R.A.: The Cambrian period. Geol. Time Scale **2012**, 437–488 (2012)
33. Fan, J.X.; Peng, S.C.; Hou, X.D.; Chen, D.Y.: Official website of the International Commission on Stratigraphy and the release of the international chronostratigraphic chart (V2015/01). J. Stratigr. **39**(2), 125–134 (2015). **(in Chinese with English abstract)**
34. Xiao, E.Z.; Sui, M.Y.; Qin, Y.L.; Latif, K.; Riaz, M.: Sequence-stratigraphy division of Cambrian in Qijiayu section. Pet. Geol. Oilfield Dev. Daqing **36**(6), 16–26 (2017). **(in Chinese with English abstract)**
35. Xiao, E.Z.; Qin, Y.L.; Riaz, M.; Latif, K.; Yao, L.; Wang, H.: Sequence stratigraphy division of Cambrian in the northeast area of Lvliang mountain: a case study of the Cangerhui section in Wenshui City. J. Northeast Pet. Univ. **41**(5), 1–19 (2017). **(in Chinese with English abstract)**
36. Latif, K.; Xiao, E.Z.; Riaz, M.; Wang, L.; Khan, M.Y.; Hussein, A.A.; Khan, M.U.: Sequence stratigraphy, sea-level changes and depositional systems in the Cambrian of the North China Platform: a case study of Kouquan section, Shanxi Province, China. J. Himal. Earth Sci. **51**(1), 1–16 (2018)
37. Riaz, M.; Latif, K.; Zafar, T.; Xiao, E.Z.; Ghazi, S.; Wang, L.; Hussein, A.A.A.: Assessment of Cambrian sequence stratigraphic style of the North China Platform exposed in Wuhai division, Inner Mongolia. Himal. Geol. **40**(1), 92–102 (2019)
38. Riaz, M.; Xiao, E.Z.; Latif, K.; Zafar, T.: Sequence-stratigraphic position of oolitic bank of Cambrian in North China Platform: example from the Kelan Section of Shanxi Province. Arab. J. Sci. Eng. **44**(1), 391–407 (2019)
39. Boulila, S.; Galbrun, B.; Miller, K.G.; Pekar, S.F.; Browning, J.L.; Laskar, J.; Wright, J.D.: On the origin of Cenozoic and

Mesozoic "third-order" eustatic sequences. Earth Sci. Rev. **109**(3–4), 94–112 (2011)
40. Riding, R.: Calcified cyanobacteria. In: Reitner, J., Thiel, V. (eds.) Encyclopedia of Geobiology. Encyclopedia of Earth Science Series, pp. 211–223. Springer, Berlin (2011)
41. Latif, K.; Xiao, E.Z.; Riaz, M.; Hussein, A.A.A.: Calcified cyanobacteria fossils from the leiolitic bioherm in the Furongian Changshan Formation, Datong (North China Platform). Carbonate Evaporite. **34**, 825–843 (2019)
42. Xiao, E.Z.; Latif, K.; Riaz, M.; Qing, Y.L.; Wang, H.: Calcified microorganisms bloom in Furongian of the North China Platform: evidence from Microbialitic-Bioherm in Qijiayu section, Hebei. Open Geosci. **10**, 250–260 (2018)
43. Xiao, E.Z.; Sui, M.Y.; Latif, K.: Riaz M (2017c) Study advances and existed problem for the forming mechanism of the microbial dolomite. Pet. Geol. Oilfield Dev. Daqing **36**(6), 16–26 (2017). **(in Chinese with English abstract)**
44. Challands, T.; Armstrong, H.; Maloney, D.P.; Davies, J.R.; Wilson, D.; Owen, A.W.: Organic-carbon deposition and coastal upwelling at mid-latitude during the Upper Ordovician (Late Katian): a case study from the Welsh Basin, UK. Palaeogeogr. Palaeoclim. **273**(3), 395–410 (2009)
45. Calvert, S.E.; Pedersen, T.F.: Geochemistry of recent oxic and anoxic marine sediments; implications for the geological record. Mar. Geol. **113**(1–2), 67–88 (1993)
46. Jones, B.; Manning, D.C.: Comparison of geochemical indices used for the interpretation of paleo-redox conditions in Ancient mudstones. Chem. Geol. **111**(1–4), 111–129 (1994)
47. Rimmer, S.M.: Geochemical paleoredox indicators in Devonian–Mississippian black shales, Central Appalachian Basin (USA). Chem. Geol. **206**, 373–391 (2004)
48. Fouke, B.W.; Schlager, W.; Vandamme, M.G.; Henderiks, J.; Van Hilten, B.: Basin-to-platform chemostratigraphy and diagenesis of the Early Cretaceous Vercors Carbonate Platform, SE France. Sediment. Geol. **175**(1–4), 297–314 (2005)
49. Tripati, A.K.; Allmon, W.D.; Sampson, D.E.: Possible evidence for a large decrease in seawater strontium/calcium ratios and strontium concentrations during the Cenozoic. Earth Planet. Sci. Lett. **282**(1), 122–130 (2009)
50. Ni, T.; Corcoran, D.L.; Rach, E.A.; Song, S.; Spana, E.P.; Gao, Y.; Zhu, J.: A paired-end sequencing strategy to map the complex landscape of transcription initiation. Nat. Methods **7**(7), 521–527 (2010)
51. Deng, C.; Thomas, K.R.; Capecchi, M.R.: Location of crossovers during gene targeting with insertion and replacement vectors. Am. Soc. Microbiol. **13**(4), 2134–2140 (1993)
52. Chen, J.; Liu, G.; Jiang, M.; Chou, C.L.; Li, H.; Wu, B.; Zheng, L.; Jiang, D.: Geochemistry of environmentally sensitive trace elements in Permian coals from the Huainan coalfield, Anhui, China. Int. J. Coal Geol. **88**(1), 41–54 (2011)
53. Dill, H.G.; Altangerel, S.; Bulgamaa, J.; Hongor, O.; Khishigsuren, S.; Majigsuren, Y.; Myagmarsuren, S.; Heunisch, C.: The Baganuur coal deposit, Mongolia: depositional environments and paleoecology of a Lower Cretaceous coal-bearing intermontane basin in Eastern Asia. Int. J. Coal Geol. **60**(2), 197–236 (2004)
54. Wignall, P.B.: Black Shales. Oxford University Press, Oxford (1994)
55. Bellanca, A.; Masetti, D.; Neri, R.: Rare earth elements in limestone/marlstone couplets from the Albian-Cenomanian Cismon section (Venetian region, northern Italy): assessing REE sensitivity to environmental changes. Chem. Geol. **141**, 141–152 (1997)
56. Haskin, L.A.; Gehl, M.A.: The rare earth distribution in sediment. J. Geophys. Res. **67**, 2537–2541 (1962)
57. Wang, Z.G.; Yu, X.Y.; Zhao, Z.H.: Progress in geochemistry of rare earth elements abroad. Bull. Mineral. Pet. Geochem. **1**, 1–4 (1986). **(in Chinese)**
58. McLennan, S.M.: Rare earth elements in sedimentary rocks: influence of provenance and sedimentary processes. Mineral. Soc. Am. **21**, 169–200 (1989)
59. Shields, G.; Stille, P.D.: Diagenetic constrains on the use of cerium anomalies as paleoseawater redox proxies: an isotopic and REE study of Cambrian phosphorites. Chem. Geol. **175**, 29–48 (2001)
60. Xu, X.; Wang, K.; Zhang, K.; Ma, Q.; Xing, L.; Sullivan, C.; Hu, D.; Cheng, S.; Wang, S.: A gigantic feathered dinosaur from the Lower Cretaceous of China. Nature **484**(7392), 92–95 (2012)
61. Nozaki, Y.: A fresh look at element distribution the North Pacific Ocean. EOS Trans. AGU **78**, 221 (1997)
62. Nozaki, Y.; Alibo, D.S.: Importance of vertical geochemical processes in controlling the oceanic profiles of dissolved rare earth elements in the northeastern Indian Ocean. Earth Planet. Sci. Lett. **205**(3–4), 155–172 (2003)
63. Hu, J.J.; Li, Q.; Li, J.; Kong, X.; Liu, Y.: Geochemical characteristics and its application to depositional environment analysis of Permian Carbonates in Jiaomuri Area, Qiangtang Basin. Geol. J. China Univ. **20**(4), 520–527 (2014). **(in Chinese with English abstract)**
64. Bau, M.; Koschinsky, A.; Dulski, P.; Hein, J.R.: Comparison of partitioning behaviors of yttrium, rare earth elements, and titanium between hydrogenetic marine ferromanganese crusts and seawater. Geochim. Cosmochim. Acta **60**, 1709–1725 (1996)
65. Nagarajan, R.; Madhavaraju, J.; Armstrong-Altrin, J.S.; Nagendra, R.: Geochemistry of Neoproterozoic limestones of the Shahabad Formation, Bhima Basin, Karnataka, southern India. Geosci. J. **15**(1), 9–25 (2011)
66. Webb, G.E.; Kamber, B.S.: Rare earth elements in Holocene reefal microbialites: a new shallow seawater proxy. Geochim. Cosmochim. Acta **64**, 1557–1565 (2000)
67. Gromet, L.P.; Haskin, L.A.; Korotev, R.L.; Dymek, R.F.: The "North American Shale Composite": its compilation, major and trace element characteristics. Geochim. Cosmochim. Acta **48**(12), 2469–2482 (1984)
68. Taylor, S.R.; McLennan, S.M.: The Continental Crust: Its Composition and Evolution. Blackwell, Oxford (1985)
69. Tanaka, K.; Miura, N.; Asahara, Y.; Kawabe, I.: Rare earth element and strontium isotopic study of seamount—type limestone in Mesozoic accretionary complex of Southern Chichibu Terrane, central Japan: implication for incorporation process of seawater REE into limestones. Geochem. J. **37**, l63–180 (2003)
70. Nothdurft, L.D.; Webb, G.E.; Kamber, B.S.: Rare earth element geochemistry of Late Devonian reefal carbonates, Canning Basin, Western Australia: confirmation of a seawater REE proxy in ancient limestones. Geochim. Cosmochim. Acta **68**(2), 263–283 (2004)
71. Baar, H.J.W.; German, C.R.; Elderfield, H.; Gaans, P.V.: Rare earth element distributions in anoxic waters of the Cariaco trench. Geochim. Cosmochim. Acta **52**, 1203–1219 (1988)
72. Yuhang, W.; Yuanyuan, Z.; Jiandong, H.; Huyue, S.; Yong, D.; Zhe, L.: Application of rare earth elements of the marine carbonate rocks in the paleoenvironmental researches. Advance Earth. Sci. **33**(9), 922–932 (2018). **(in Chinese with English abstract)**
73. Piper, D.Z.: Rare earth elements in the sedimentary cycle: a summary. Chem. Geol. **14**(4), 285–304 (1974)
74. Elderfield, H.; Greaves, M.J.: The rare earth elements in seawater. Nature **296**, 214–219 (1982)
75. German, C.R.; Elderfield, H.: Rare earth elements in the NW Indian Ocean. Geochim. Cosmochim. Acta **54**, 1929–1940 (1990)
76. Michard, A.; Albarede, F.: The REE content of some hydrothermal fluids. Chem. Geol. **55**(1–2), 21–60 (1986)
77. Kamber, B.S.; Bolhar, R.; Webb, G.E.: Geochemistry of late Archaean stromatolites from Zimbabwe: evidence for microbial

life in restricted epicontinental seas. Precambrian Res. **132**, 379–399 (2004)
78. Bau, M.; Dulski, P.: Distribution of yttrium and rare-earth elements in the Penge and Kuruman iron-formations, Transvaal Supergroup, South Africa. Precambrian Res. **79**(1–2), 37–55 (1996)
79. Sholkovitz, E.R.; Landing, W.M.; Lewis, B.L.: Ocean particle chemistry: the fractionation of rare earth elements between suspended particles and seawater. Geochim. Cosmochim. Acta **58**, 1567–1580 (1994)
80. Krumbein, W.E.; Cohen, Y.; Shilo, M.: Solar Lake (Sinai). 4. Stromatolitic cyanobacterial mats. Limnol. Oceanogr. **22**(4), 635–656 (1977)
81. Gerdes, G.; Dunajtschik-Piewak, K.; Riege, H.; Taher, A.G.; Krumbein, W.E.; Reineck, H.E.: Structural diversity of biogenic carbonate particles in microbial mats. Sedimentology **41**, 1273–1294 (1994)
82. Baumgartner, L.K.; Reid, R.P.; Dupraz, C.; Decho, A.W.; Buckley, D.H.; Spear, J.R.; Przekop, K.M.; Visscher, P.T.: Sulfate reducing bacteria in microbial mats: changing paradigms, new discoveries. Sediment. Geol. **185**(3), 131–145 (2006)
83. Mei, M.; Yang, F.; Gao, J.; Meng, Q.F.: Glauconites formed in the high-energy shallow-marine environment of the Late Mesoproterozoic: case study from Tieling Formation at Jixian Section in Tianjin, North China. Earth Sci. Front. **15**(4), 146–158 (2008)
84. Gallagher, M.; Turner, E.C.; Kamber, B.S.: In situ trace metal analysis of Neoarchaean–Ordovician shallow-marine microbial-carbonate-hosted pyrites. Geobiology **13**(4), 316–339 (2015)
85. Canfield, D.E.: A new model for Proterozoic ocean chemistry. Nature **396**, 450–453 (1998)
86. Bratton, J.F.; Berry, W.B.N.; Morrow, J.R.: Anoxia pre-dates Frasnian–Famennian boundary mass extinction horizon in the Great Basin, USA. Palaeogeogr. Palaeoclim. **154**, 275–292 (1999)
87. Turgeon, S.; Brumsack, H.: Anoxic versus dysoxic events reflected in sediment geochemistry during the Cenomanian–Turonian Boundary Event (Cretaceous) in the Umbria–Marche Basin of central Italy. Chem. Geol. **234**(3), 321–339 (2006)
88. Tribovillard, N.; Algeo, T.J.; Lyons, T.; Riboulleau, A.: Trace metals as paleoredox and paleoproductivity proxies: an update. Chem. Geol. **232**(1–2), 12–32 (2006)
89. Li, S.Y.; Jin, F.Q.; Wang, D.X.: Geochemical characteristics of carbonate rock diagenesis. Exper. Petrol. Geol. **17**(1), 55–61 (1995). **(in Chinese with English abstract)**
90. Chen, S.; Fu, X.H.; Gui, H.R.; Sun, L.H.: Geochemical characteristics of trace elements in limestone of the Neoproterozoic Wangshan Formation in northern Anhui Province. J. Palaeogeogr. **14**(6), 813–820 (2012)
91. Ma, Y.S.; Mei, M.X.; Zhou, R.X.; Yang, W.: Forming patterns for the oolitic bank within the sequence-stratigraphic framework: an example from the Cambrian Series 3 at the Xiaweidian section in the western suburb of Beijing. Acta Pet. Sin. **33**(4), 1021–1036 (2017). **(in Chinese with English abstract)**